
Towards Biologically Plausible Convolutional Networks

Roman Pogodin
Gatsby Unit, UCL
roman.pogodin.17@ucl.ac.uk

Yash Mehta
Gatsby Unit, UCL
y.mehta@ucl.ac.uk

Timothy P. Lillicrap
DeepMind; CoMPLEX, UCL
countzero@google.com

Peter E. Latham
Gatsby Unit, UCL
pel@gatsby.ucl.ac.uk

Abstract

Convolutional networks are ubiquitous in deep learning. They are particularly useful for images, as they reduce the number of parameters, reduce training time, and increase accuracy. However, as a model of the brain they are seriously problematic, since they require weight sharing – something real neurons simply cannot do. Consequently, while neurons in the brain can be locally connected (one of the features of convolutional networks), they cannot be convolutional. Locally connected but non-convolutional networks, however, significantly underperform convolutional ones. This is troublesome for studies that use convolutional networks to explain activity in the visual system. Here we study plausible alternatives to weight sharing that aim at the same regularization principle, which is to make each neuron within a pool react similarly to identical inputs. The most natural way to do that is by showing the network multiple translations of the same image, akin to saccades in animal vision. However, this approach requires many translations, and doesn't remove the performance gap. We propose instead to add lateral connectivity to a locally connected network, and allow learning via Hebbian plasticity. This requires the network to pause occasionally for a sleep-like phase of "weight sharing". This method enables locally connected networks to achieve nearly convolutional performance on ImageNet and improves their fit to the ventral stream data, thus supporting convolutional networks as a model of the visual stream.

1 Introduction

Convolutional networks are a cornerstone of modern deep learning: they're widely used in the visual domain [1, 2, 3], speech recognition [4], text classification [5], and time series classification [6]. They have also played an important role in enhancing our understanding of the visual stream [7]. Indeed, simple and complex cells in the visual cortex [8] inspired convolutional and pooling layers in deep networks [9] (with simple cells implemented with convolution and complex ones with pooling). Moreover, the representations found in convolutional networks are similar to those in the visual stream [10, 11, 12, 13] (see [7] for an in-depth review).

Despite the success of convolutional networks at reproducing activity in the visual system, as a model of the visual system they are somewhat problematic. That's because convolutional networks share weights, something biological networks, for which weight updates must be local, can't do [14]. Locally connected networks avoid this problem by using the same receptive fields as convolutional networks (thus locally connected), but without weight sharing [15]. However, they pay a price for biological plausibility: locally connected networks are known to perform worse than their

convolutional counterparts on hard image classification tasks [15, 16]. There is, therefore, a need for a mechanism to bridge the gap between biologically plausible locally connected networks and implausible convolutional ones.

Here, we consider two such mechanisms. One is to use extensive data augmentation (primarily image translations); the other is to introduce an auxiliary objective that allows some form of weight sharing, which is implemented by lateral connections; we call this approach dynamic weight sharing.

The first approach, data augmentation, is simple, but we show that it suffers from two problems: it requires far more training data than is normally used, and even then it fails to close the performance gap between convolutional and locally connected networks. The second approach, dynamic weight sharing, implements a sleep-like phase in which neural dynamics facilitate weight sharing. This is done through lateral connections in each layer, which allows subgroups of neurons to share their activity. Through this lateral connectivity, each subgroup can first equalize its weights via anti-Hebbian learning, and then generate an input pattern for the next layer that helps it to do the same thing. Dynamic weight sharing doesn't achieve perfectly convolutional connectivity, because in each channel only subgroups of neurons share weights. However, it implements a similar inductive bias, and, as we show in experiments, it performs almost as well as convolutional networks, and also achieves better fit to the ventral stream data, as measured by the Brain-Score [12, 17].

Our study suggests that convolutional networks may be biologically plausible, as they can be approximated in realistic networks simply by adding lateral connectivity and Hebbian learning. As convolutional networks and locally connected networks with dynamic weight sharing have similar performance, convolutional networks remain a good "model organism" for neuroscience. This is important, as they consume much less memory than locally connected networks, and run much faster.

2 Related work

Studying systems neuroscience through the lens of deep learning is an active area of research, especially when it comes to the visual system [18]. As mentioned above, convolutional networks in particular have been extensively studied as a model of the visual stream (and also inspired by it) [7], and also as mentioned above, because they require weight sharing they lack biological plausibility. They have also been widely used to evaluate the performance of different biologically plausible learning rules [15, 19, 20, 21, 22, 23, 24, 25].

Several studies have tried to relax weight sharing in convolutions by introducing locally connected networks [15, 16, 26] ([26] also shows that local connectivity itself can be learned from a fully connected network with proper weight regularization). Locally connected networks perform as well as convolutional ones in shallow architectures [15, 26]. However, they perform worse for large networks and hard tasks, unless they're initialized from an already well-performing convolutional solution [16] or have some degree of weight sharing [27]. In this study, we seek biologically plausible regularizations of locally connected network to improve their performance.

Convolutional networks are not the only deep learning architecture for vision: visual transformers (e.g., [28, 29, 30, 31]), and more recently, the transformer-like architectures without self-attention [32, 33, 34], have shown competitive results. However, they still need weight sharing: at each block the input image is reshaped into patches, and then the same weight is used for all patches. Our Hebbian-based approach to weight sharing fits this computation as well (see Appendix A.4).

3 Regularization in locally connected networks

3.1 Convolutional versus locally connected networks

Convolutional networks are implemented by letting the weights depend on the difference in indices. Consider, for simplicity, one dimensional convolutions and a linear network. Letting the input and output of a one layer in a network be x_j and z_i , respectively, the activity in a convolutional network is

$$z_i = \sum_{j=1}^N w_{i-j} x_j, \tag{1}$$

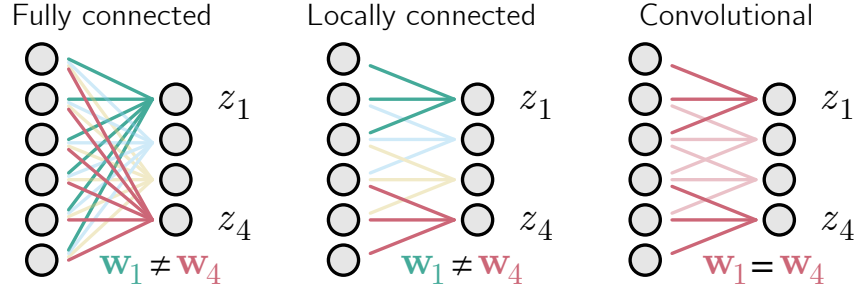


Figure 1: Comparison between layer architectures: fully connected (left), locally connected (middle) and convolutional (right). Locally connected layers have different weights for each neuron z_1 to z_4 (indicated by different colors), but have the same connectivity as convolutional layers.

where N is the number of neurons; for definiteness, we'll assume N is the same in each layer (right panel in Fig. 1). Although the index j ranges over all N neurons, many, if not most, of the weights are zero: w_{i-j} is nonzero only when $|i-j| \leq k/2 < N$ for kernel size k .

For networks that aren't convolutional, the weight matrix w_{i-j} is replaced by w_{ij} ,

$$z_i = \sum_{j=1}^N w_{ij} x_j. \quad (2)$$

Again, the index j ranges over all N neurons. If all the weights are nonzero, the network is fully connected (left panel in Fig. 1). But, as in convolutional networks, we can restrict the connectivity range by letting w_{ij} be nonzero only when $|i-j| \leq k/2 < N$, resulting in a *locally connected*, but non-convolutional, network (center panel in Fig. 1).

3.2 Developing convolutional weights: data augmentation versus dynamic weight sharing

Here we explore the question: is it possible for a locally connected network to develop approximately convolutional weights? That is, after training, is it possible to have $w_{ij} \approx w_{i-j}$? There is one straightforward way to do this: augment the data to provide multiple translations of the same image, so that each neuron within a channel learns to react similarly (Fig. 2A). A potential problem is that a large number of translations will be needed. This makes training costly (see Section 5), and is unlikely to be consistent with animal learning, as animals see only a handful of translations of any one image.

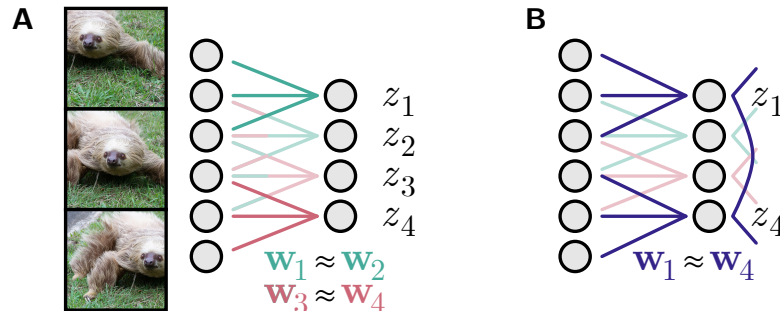


Figure 2: Two regularization strategies for locally connected networks. **A.** Data augmentation, where multiple translations of the same image are presented simultaneously. **B.** Dynamic weight sharing, where a subset of neurons equalizes their weights through lateral connections and learning.

A less obvious solution is to modify the network so that during learning the weights become approximately convolutional. As we show in the next section, this can be done by adding lateral connections, and introducing a *sleep phase* during training (Fig. 2B). This solution doesn't need more data, but it does need an additional training step.

4 A Hebbian solution to dynamic weight sharing

If we were to train a locally connected network without any weight sharing or data augmentation, the weights of different neurons would diverge (region marked “training” in Fig. 3A). Our strategy to make them convolutional is to introduce an occasional sleep phase, during which the weights relax to their mean over output neurons (region marked “sleep” in Fig. 3A). This will compensate weight divergence during learning by convergence during the sleep phase. If the latter is sufficiently strong, the weights will remain approximately convolutional.

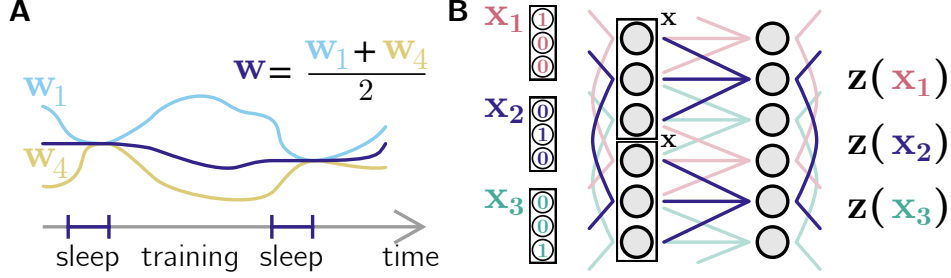


Figure 3: **A.** Dynamical weight sharing interrupts the main training loop, and equalizes the weights through internal dynamics. After that, the weights diverge again until the next weight sharing phase. **B.** A locally connected network, where both the input and the output neurons have lateral connections. The input layer uses lateral connections to generate repeated patterns for weight sharing in the output layer. For instance, the output neurons connected by the dark blue lateral connections (middle) can receive three different patterns: \mathbf{x}_1 (generated by the red input grid), \mathbf{x}_2 (dark blue) and \mathbf{x}_3 (green).

To implement this, we introduce lateral connectivity, chosen to equalize activity in both the input and output layer. That’s shown in Fig. 3B, where every third neuron in both the input (\mathbf{x}) and output (\mathbf{z}) layers are connected. Once the connected neurons in the input layer have equal activity, all output neurons receive identical input. Since the lateral output connections also equalize activity, all connection that correspond to a translation by three neurons see exactly the same pre and postsynaptic activity. A naive Hebbian learning rule (with weight decay) would, therefore, make the network convolutional. However, we have to take care that the initial weights are not over-written during Hebbian learning. We now describe how that is done.

To ease notation, we’ll let \mathbf{w}_i be a vector containing the incoming weights to neuron i : $(\mathbf{w}_i)_j \equiv w_{ij}$. Moreover, we’ll let j run from 1 to k , independent of i . With this convention, the response of neuron i , z_i , to a k -dimensional input, \mathbf{x} , is given by

$$z_i = \mathbf{w}_i^\top \mathbf{x} = \sum_{j=1}^k w_{ij} x_j. \quad (3)$$

Assume that every neuron sees the same \mathbf{x} , and consider the following update rule for the weights,

$$\Delta \mathbf{w}_i \propto - \left(z_i - \frac{1}{N} \sum_{j=1}^N z_j \right) \mathbf{x} - \gamma (\mathbf{w}_i - \mathbf{w}_i^{\text{init}}), \quad (4)$$

where $\mathbf{w}_i^{\text{init}}$ are the weights at the beginning of the sleep phase (not the overall training).

This Hebbian update effectively implements SGD over the sum of $(z_i - z_j)^2$, plus a regularizer (the second term) to keep the weights near $\mathbf{w}_i^{\text{init}}$. If we present the network with M different input vectors, \mathbf{x}_m , and denote the covariance matrix $\mathbf{C} \equiv \frac{1}{M} \sum_m \mathbf{x}_m \mathbf{x}_m^\top$, then, asymptotically, the weight dynamics in Eq. (4) converges to (see Appendix A)

$$\mathbf{w}_i^* = (\mathbf{C} + \gamma \mathbf{I})^{-1} \left(\mathbf{C} \frac{1}{N} \sum_{j=1}^N \mathbf{w}_j^{\text{init}} + \gamma \mathbf{w}_i^{\text{init}} \right) \quad (5)$$

where \mathbf{I} is the identity matrix.

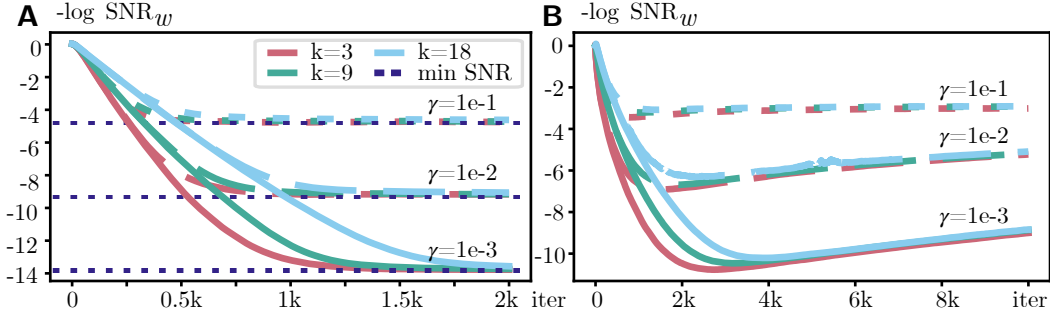


Figure 4: Negative logarithm of signal-to-noise ratio (mean weight squared over weight variance, see Eq. (6)) for weight sharing objectives in a layer with 100 neurons. Different curves have different kernel size, k (meaning k^2 inputs), and regularization parameter, γ . **A.** Weight updates given by Eq. (4). Black dashed lines show the theoretical minimum. **B.** Weight updates given by Eq. (8), with $\alpha = 10$. In each iteration, the input is presented for 150 ms.

As long as **C** is full rank and γ is small, we arrive at shared weights: $\mathbf{w}_i^* \approx \frac{1}{N} \sum_{i=1}^N \mathbf{w}_i^{\text{init}}$. It might seem advantageous to set $\gamma = 0$, as non-zero γ only biases the equilibrium value of the weight. However, non-zero γ ensures that for noisy input, $\mathbf{x}_i = \mathbf{x} + \xi_i$ (such that the inputs to different neurons are the same only on average, which is much more realistic), the weights still converge (at least approximately) to the mean of the initial weights (see Appendix A).

In practice, the dynamics in Eq. (4) converges quickly. We illustrate it in Fig. 4A by plotting $-\log \text{SNR}_w$ over time, where SNR_w , the signal to noise ratio of the weights, is defined as

$$\text{SNR}_w = \frac{1}{k^2} \sum_j \frac{\left(\frac{1}{N} \sum_i (\mathbf{w}_i)_j\right)^2}{\frac{1}{N} \sum_i \left(\frac{1}{N} \sum_{i'} (\mathbf{w}_{i'})_j\right)^2}. \quad (6)$$

For all kernel sizes (we used 2d inputs, meaning k^2 inputs per neuron), the weights converge to a nearly convolutional solution within a few hundred iterations (note the logarithmic scale of the y axis in Fig. 4A). See Appendix A for simulation details. Thus, to run our experiments with deep networks in a realistic time frame, we perform weight sharing instantly (i.e., directly setting them to the mean value) during the sleep phase.

4.1 Dynamic weight sharing in multiple locally connected layers

As shown in Fig. 3B, the k -dimensional input, \mathbf{x} , repeats every k neurons. Consequently, during the sleep phase, the weights are not set to the mean of their initial value averaged across all neurons; instead, they're set to the mean averaged across a set of neurons spaced by k . Thus, in one dimension, the sleep phase equilibrates the weights in k different modules. In two dimensions (the realistic case), the sleep phase equilibrates the weights in k^2 different modules.

We need this spacing to span the whole k -dimensional (or k^2 for 2d) space of inputs. For instance, activating the red grid on the left in Fig. 3B generates \mathbf{x}_1 , covering one input direction for all output neurons (and within each module, every neuron receives the same input). Next, activating the blue grid generates \mathbf{x}_2 (a new direction), and so on.

In multiple layers, the sleep phase is implemented layer by layer. In layer l , lateral connectivity creates repeated input patterns and feeds them to layer $l + 1$. After weight sharing in layer $l + 1$, the new pattern from $l + 1$ is fed to $l + 2$, and so on. Notably, there's no layer by layer plasticity schedule (i.e., deeper layers don't have to wait for the earlier ones to finish), as the weight decay term in Eq. (4) ensures the final solution is the same regardless of intermediate weight updates. As long as a deeper layer starts receiving repeated patterns, it will eventually arrive at the correct solution. Our approach has two limitations. First, this pattern generation scheme needs layers to have filters of the same size. Second, we assume that the very first layer (e.g., V1) receives inputs from another area (e.g., LGN) that can generate repeated patterns, but doesn't need weight sharing.

4.2 A realistic model that implements the update rule

Our update rule, Eq. (4), implies that there is a linear neuron, denoted r_i , whose activity depends on the upstream input, $z_i = \mathbf{w}_i^\top \mathbf{x}$, via a direct excitatory connection combined with lateral inhibition,

$$r_i = z_i - \frac{1}{N} \sum_{j=1}^N z_j \equiv \mathbf{w}_i^\top \mathbf{x} - \frac{1}{N} \sum_{j=1}^N \mathbf{w}_j^\top \mathbf{x}. \quad (7)$$

The resulting update rule is anti-Hebbian, $-r_i \mathbf{x}$ (see Eq. (4)). In a realistic circuit, this can be implemented with excitatory neurons r_i and an inhibitory neuron r_{inh} , which obey the dynamics

$$\tau \dot{r}_i = -r_i + \mathbf{w}_i^\top \mathbf{x} - \alpha r_{\text{inh}} + b \quad (8a)$$

$$\tau \dot{r}_{\text{inh}} = -r_{\text{inh}} + \frac{1}{N} \sum_j r_j - b, \quad (8b)$$

where b is the shared bias term that ensures non-negativity of firing rates (assuming $\sum_i \mathbf{w}_i^\top \mathbf{x}$ is positive, which would be the case for excitatory input neurons). The only fixed point of this equations is

$$r_i^* = b + \mathbf{w}_i^\top \mathbf{x} - \frac{1}{N} \sum_j \mathbf{w}_j^\top \mathbf{x} + \frac{1}{1 + \alpha} \frac{1}{N} \sum_j \mathbf{w}_j^\top \mathbf{x} \underset{\alpha \gg 1}{\approx} b + \mathbf{w}_i^\top \mathbf{x} - \frac{1}{N} \sum_j \mathbf{w}_j^\top \mathbf{x}, \quad (9)$$

which is stable. As a result, for strong inhibition ($\alpha \gg 1$), Eq. (4) can be implemented with an anti-Hebbian term $-(r_i - b)\mathbf{x}$. Note that if $\mathbf{w}_i^\top \mathbf{x}$ is zero on average, then b is the mean firing rate over time. To show that Eq. (9) provides enough signal, we simulated training in a network of 100 neurons that receives a new \mathbf{x} each 150 ms. For a range of k and γ , it converged to a nearly convolutions solution within minutes (Fig. 4B; each iteration is 150 ms). Having finite inhibition did lead to worse final signal-to-noise ration ($\alpha = 10$ in Fig. 4B), but the variance of the weights was still very small. Moreover, the nature of the α -induced bias suggests that stopping training before convergence leads to better results (around 2k iterations in Fig. 4B). See Appendix A for a discussion.

5 Experiments

We split our experiments into two parts: small-scale ones with CIFAR10, CIFAR100 [35] and TinyImageNet [36], and large-scale ones with ImageNet [37]. The former illustrates the effects of data augmentation and dynamic weight sharing on the performance of locally connected networks; the latter concentrates on dynamic weight sharing, as extensive data augmentations are too computationally expensive for large networks and datasets. We used the AdamW [38] optimizer in all runs. As our dynamic weight sharing procedure always converges to a nearly convolutional solution (see Section 4), we set the weights to the mean directly (within each grid) to speed up experiments. Our code is available at <https://github.com/romanpogodin/towards-bio-plausible-conv> (PyTorch [39] implementation).

Datasets. CIFAR10 consists of 50k training and 10k test images of size 32×32 , divided into 10 classes. CIFAR100 has the same structure, but with 100 classes. For both, we tune hyperparameters with a 45k/5k train/validation split, and train final networks on the full 50k training set. TinyImageNet consists of 100k training and 10k validation images of size 64×64 , divided into 200 classes. As the test labels are not publicly available, we divided the training set into 90k/10k train/validation split, and used the 10k official validation set as test data. ImageNet consists of 1.281 million training images and 50k test images of different sizes, reshaped to 256 pixels in the smallest dimension. As in the case for TinyImageNet, we used the train set for a 1.271 million/10k train/validation split, and 50k official validation set as test data.

Networks. For CIFAR10/100 and TinyImageNet, we used CIFAR10-adapted ResNet20 from the original ResNet paper [3]. The network has three blocks, each consisting of 6 layers, with 16/32/64 channels within the block. We chose this network due to good performance on CIFAR10, and the ability to fit the corresponding locally connected network into the 8G VRAM of the GPU for large batch sizes on all three datasets. For ImageNet, we took the half-width ResNet18 (meaning 32/64/128/256 block widths) to be able to fit a common architecture (albeit halved in width) in the locally connected regime into 16G of GPU VRAM. For both networks, all layers had 3×3 receptive

Table 1: Performance of convolutional (conv) and locally connected (LC) networks for padding of 4 in the input images (mean accuracy over 5 runs). For LC, two regularization strategies were applied: repeating the same image n times with different translations (n reps) or using dynamic weight sharing every n batches ($ws(n)$). LC nets additionally show performance difference w.r.t. conv nets.

Regularizer	Connectivity	CIFAR10		CIFAR100		TinyImageNet					
		Top-1 accuracy (%)	Diff	Top-1 accuracy (%)	Diff	Top-5 accuracy (%)	Diff	Top-1 accuracy (%)	Diff	Top-5 accuracy (%)	Diff
-	conv	88.3	-	59.2	-	84.9	-	38.6	-	65.1	-
	LC	80.9	-7.4	49.8	-9.4	75.5	-9.4	29.6	-9.0	52.7	-12.4
Data Translation	LC - 4 reps	82.9	-5.4	52.1	-7.1	76.4	-8.5	31.9	-6.7	54.9	-10.2
	LC - 8 reps	83.8	-4.5	54.3	-5.0	77.9	-7.0	33.0	-5.6	55.6	-9.5
	LC - 16 reps	85.0	-3.3	55.9	-3.3	78.8	-6.1	34.0	-4.6	56.2	-8.8
Weight Sharing	LC - ws(1)	87.4	-0.8	58.7	-0.5	83.4	-1.6	41.6	3.0	66.1	1.1
	LC - ws(10)	85.1	-3.2	55.7	-3.6	80.9	-4.0	37.4	-1.2	61.8	-3.2
	LC - ws(100)	82.0	-6.3	52.8	-6.4	80.1	-4.8	37.1	-1.5	62.8	-2.3

field (apart from a few 1×1 residual downsampling layers), meaning that weight sharing worked over 9 individual grids in each layer.

Training details. We ran the experiments on our local laboratory cluster, which consists mostly of NVIDIA GTX1080 and RTX5000 GPUs. The small-scale experiments took from 1-2 hours per run up to 40 hours (for TinyImageNet with 16 repetitions). The large-scale experiments took from 3 to 6 days on RTX5000 (the longest run was the locally connected network with weight sharing happening after every minibatch update).

5.1 Data augmentations.

For CIFAR10/100, we padded the images (padding size depended on the experiment) with mean values over the training set (such that after normalization the padded values were zero) and cropped to size 32×32 . We did not use other augmentations to separate the influence of padding/random crops. For TinyImageNet, we first center-cropped the original images to size $(48 + 2 \text{ pad}) \times (48 + 2 \text{ pad})$ for the chosen padding size pad. The final images were then randomly cropped to 48×48 . This was done to simulate the effect of padding on the number of available translations, and to compare performance across different padding values on the images of the same size (and therefore locally connected networks of the same size). After cropping, the images were normalized using ImageNet normalization values. For all three datasets, test data was sampled without padding. For ImageNet, we used the standard augmentations. Training data was resized to 256 (smallest dimension), random cropped to 224×224 , flipped horizontally with 0.5 probability, and then normalized. Test data was resized to 256, center cropped to 224 and then normalized. In all cases, data repetitions included multiple samples of the same image within a batch, keeping the total number of images in a batch fixed (e.g. for batch size 256 and 16 repetitions, that would mean 16 original images)

5.2 CIFAR10/100 and TinyImageNet

To study the effect of both data augmentation and weight sharing on performance, we ran experiments with non-augmented images (padding 0) and with different amounts of augmentations. This included padding of 4 and 8, and repetitions of 4, 8, and 16. Without augmentations, locally connected networks performed much worse than convolutional, although weight sharing improved the result a little bit (see Appendix B). For padding of 4 (mean accuracy over 5 runs Table 1, see Appendix B for max-min accuracy), increasing the number of repetitions increased the performance of locally connected networks. However, even for 16 repetitions, the improvements were small comparing to weight sharing (especially for top-5 accuracy on TinyImageNet). For CIFAR10, our results are consistent with an earlier study of data augmentations in locally connected networks [40]. For dynamic weight sharing, doing it moderately often – every 10 iterations, meaning every 5120 images – did as well as 16 repetitions on CIFAR10/100. For TinyImageNet, sharing weights every 100 iterations (about every 50k images) performed much better than data augmentation.

Sharing weights after every batch performed almost as well as convolutions (and even a bit better on TinyImageNet, although the difference is small if we look at top-5 accuracy, which is a less volatile metric for 200 classes), but it is too frequent to be a plausible sleep phase. We include it to show that best possible performance of partial weight sharing is comparable to actual convolutions.

Table 2: Performance of convolutional (conv) and locally connected (LC) networks on ImageNet for 0.5x width ResNet18 (1 run). For LC, we also used dynamic weight sharing every n batches. LC nets additionally show performance difference w.r.t. the conv net.

Connectivity	Weight sharing frequency	ImageNet			
		Top-1 accuracy (%)	Diff	Top-5 accuracy (%)	Diff
conv	-	63.5	-	84.7	-
LC	-	46.7	-16.8	70.0	-14.7
LC	1	61.7	-1.8	83.1	-1.6
LC	10	59.3	-4.2	81.1	-3.6
LC	100	54.5	-9.0	77.7	-7.0

For a padding of 8, the performance did improve for all methods (including convolutions), but the relative differences had a similar trend as for a padding of 4 (see Appendix B). We also trained locally connected networks with one repetition, but for longer and with a much smaller learning rate to simulate the effect of data repetitions. Even for 4x-8x longer runs, the networks barely matched the performance of a 1-repetition network on standard speed (not shown).

5.3 ImageNet

On ImageNet, we did not test image repetitions due to the computational requirements (e.g., running 16 repetitions with our resources would take almost 3 months). We used the standard data augmentation, meaning that all networks see different crops of the same image throughout training.

Our results are shown in Table 2. Weight sharing every 1 and 10 iterations (256/2560 images, respectively, for the batch size of 256) achieves nearly convolutional performance, although less frequent weight sharing results in a more significant performance drop. In contrast, the purely locally connected network has a large performance gap with respect to the convolutional one. It is worth noting that the trade-off between weight sharing frequency and performance depends on the learning rate, as weights diverge less for smaller learning rates. It should be possible to decrease the learning rate and increase the number of training epochs, and achieve comparable results with less frequent weight sharing.

5.4 Brain-Score of ImageNet-trained networks

In addition to ImageNet performance, we evaluated how well representations built by our networks correspond to ventral stream data in primates. For that we used the Brain-Score [12, 17], a set of metrics that evaluate deep networks’ correspondence to neural recordings of cortical areas V1 [41, 42], V2 [41], V4 [43], and inferior temporal (IT) cortex [43] in primates, as well as behavioral data [44]. The advantage of Brain-Score is that it provides a standardized benchmark that looks at the whole ventral stream, and not only its isolated properties like translation invariance (which many early models focused on [45, 46, 47, 48]). We do not directly check for translation invariance in our models (only through V1/V2 data). However, as our approach achieves convolutional solutions (see above), we trivially have translation equivariance after training: translating the input will translate the layer’s response (in our case, each k -th translation will produce the same translated response for a kernel of size k). (In fact, it’s pooling layers, not convolutions, that achieve some degree of invariance in convolutional networks – this is an architectural choice and is somewhat tangential to our problem.)

Our results are shown in Table 3 (higher is better; see <http://www.brain-score.org/> for the scores of other models). The well-performing locally connected networks (with weight sharing/sleep phase every 1 or 10 iterations) show overall better fit compared to their fully convolutional counterpart – meaning that plausible approximations to convolutions also form more realistic representations. Interestingly, the worst-performing purely locally connected network had the second best V1 fit, despite overall poor performance.

In general, Brain-Score correlates with ImageNet performance (Fig. 2 in [12]). This means that the worse Brain-Score performance of the standard locally connected network and the one with weight sharing every 100 iterations can be related to their poor ImageNet performance (Table 2). (It also means that our method can potentially increase Brain-Score performance of larger models.)

Table 3: Brain-Score of ImageNet-trained convolutional (conv) and locally connected (LC) networks on ImageNet for 0.5x width ResNet18 (higher is better). For LC, we also used dynamic weight sharing every n batches. *The models were evaluated on Brain-Score benchmarks available during submission. If new benchmarks are added and the models are re-evaluated on them, the final scores might change; the provided links contain the latest results.

Connectivity	Weight sharing frequency	Brain-Score						
		average score	V1	V2	V4	IT	behavior	link*
conv	-	.357	.493	.313	.459	.370	.148	brain-score.org/model/876
LC	-	.349	.542	.291	.448	.354	.108	brain-score.org/model/877
LC	1	.396	.512	.339	.468	.406	.255	brain-score.org/model/880
LC	10	.385	.508	.322	.478	.399	.216	brain-score.org/model/878
LC	100	.351	.523	.293	.467	.370	.101	brain-score.org/model/879

6 Discussion

We presented two ways to circumvent the biological implausibility of weight sharing, a crucial component of convolutional networks. The first was through data augmentation via multiple image translations. The second was dynamic weight sharing via lateral connections, which allows neurons to share weight information during a sleep-like phase; weight updates are then done using Hebbian plasticity. Data augmentation requires a large number of repetitions in the data, and, consequently, longer training times, and yields only small improvements in performance. However, only a small number of repetitions can be naturally covered by saccades. Dynamic weight sharing needs a separate sleep phase, rather than more data, and yields large performance gains. In fact, it achieves near convolutional performance even on hard tasks, such as ImageNet classification, making it a much more likely candidate than data augmentation for the brain. In addition, well-performing locally connected networks trained with dynamic weight sharing achieve a better fit to the ventral stream data (measured by the Brain-Score [12, 17]). The sleep phase can occur during actual sleep, when the network (i.e., the visual system) stops receiving visual inputs, but maintains some internal activity. This is supported by plasticity studies during sleep (e.g. [49, 50]).

There are several limitations to our implementation of dynamic weight sharing. First, it relies on precise lateral connectivity. This can be genetically encoded, or learned early on using correlations in the input data (if layer l can generate repeated patterns, layer $l + 1$ can modify its lateral connectivity based on input correlations). Lateral connections do in fact exist in the visual stream, with neurons that have similar tuning curves showing strong lateral connections [51]. Second, the sleep phase works iteratively over layers. This can be implemented with neuromodulation that enables plasticity one layer at a time. Alternatively, weight sharing could work simultaneously in the whole network due to weight regularization (as it ensures that the final solution preserves the initial average weight), although this would require longer training due to additional noise in deep layers. Third, in our scheme the lateral connections are used only for dynamic weight sharing, and not for training or inference. As our realistic model in Section 4.2 implements this connectivity via an inhibitory neuron, we can think of that neuron as being silent outside of the sleep phase. Finally, we trained networks using backpropagation, which is not biologically plausible [18]. However, our weight sharing scheme is independent of the wake-phase training algorithm, and therefore can be applied along with any biologically plausible update rule.

Our approach to dynamic weight sharing is not relevant only to convolutions. First, it is applicable to non-convolutional networks, and in particular visual transformers [28, 29, 30, 31] (and more recent MLP-based architectures [32, 33, 34]). In such architectures, input images (and intermediate two-dimensional representations) are split into non-overlapping patches; each patch is then transformed with the *same* fully connected layer – a computation that would require weight sharing in the brain. This can be done by connecting neurons across patches that have the same relative position, and applying our weight dynamics (see Appendix A.4). Second, [23] faced a problem similar to weight sharing – weight transport (i.e., neurons not knowing their output weights) – when developing a plausible implementation of backprop. Their weight mirror algorithms used an idea similar to ours: the value of one weight was sent to another through correlations in activity.

Our study shows that both performance and the computation of convolutional networks can be reproduced in more realistic architectures. This supports convolutional networks as a model of the

visual stream, and also justifies them as a “model organism” for studying learning in the visual stream (which is important partially due to their computational efficiency). While our study does not have immediate societal impacts (positive or negative), it further strengthens the role of artificial neural networks as a model of the brain. Such models can guide medical applications such as brain machine interfaces and neurological rehabilitation. However, that could also lead to the design of potentially harmful adversarial attacks on the brain.

Acknowledgments and Disclosure of Funding

The authors would like to thank Martin Schrimpf and Mike Ferguson for their help with the Brain-Score evaluation.

This work was supported by the Gatsby Charitable Foundation, the Wellcome Trust and DeepMind.

References

- [1] Alex Krizhevsky, Ilya Sutskever, and Geoffrey E Hinton. Imagenet classification with deep convolutional neural networks. *Advances in neural information processing systems*, 25:1097–1105, 2012.
- [2] Karen Simonyan and Andrew Zisserman. Very deep convolutional networks for large-scale image recognition. *arXiv preprint arXiv:1409.1556*, 2014.
- [3] Kaiming He, Xiangyu Zhang, Shaoqing Ren, and Jian Sun. Deep residual learning for image recognition. In *Proceedings of the IEEE conference on computer vision and pattern recognition*, pages 770–778, 2016.
- [4] Ossama Abdel-Hamid, Abdel-rahman Mohamed, Hui Jiang, Li Deng, Gerald Penn, and Dong Yu. Convolutional neural networks for speech recognition. *IEEE/ACM Transactions on audio, speech, and language processing*, 22(10):1533–1545, 2014.
- [5] Alexis Conneau, Holger Schwenk, Loïc Barrault, and Yann Lecun. Very deep convolutional networks for text classification. *arXiv preprint arXiv:1606.01781*, 2016.
- [6] Fazle Karim, Somshubra Majumdar, Houshang Darabi, and Shun Chen. Lstm fully convolutional networks for time series classification. *IEEE access*, 6:1662–1669, 2017.
- [7] Grace W. Lindsay. Convolutional Neural Networks as a Model of the Visual System: Past, Present, and Future. *Journal of Cognitive Neuroscience*, pages 1–15, 02 2020.
- [8] David H Hubel and Torsten N Wiesel. Receptive fields, binocular interaction and functional architecture in the cat’s visual cortex. *The Journal of physiology*, 160(1):106–154, 1962.
- [9] Kunihiko Fukushima and Sei Miyake. Neocognitron: A self-organizing neural network model for a mechanism of visual pattern recognition. In *Competition and cooperation in neural nets*, pages 267–285. Springer, 1982.
- [10] Daniel LK Yamins, Ha Hong, Charles F Cadieu, Ethan A Solomon, Darren Seibert, and James J DiCarlo. Performance-optimized hierarchical models predict neural responses in higher visual cortex. *Proceedings of the national academy of sciences*, 111(23):8619–8624, 2014.
- [11] Seyed-Mahdi Khaligh-Razavi and Nikolaus Kriegeskorte. Deep supervised, but not unsupervised, models may explain it cortical representation. *PLoS computational biology*, 10(11):e1003915, 2014.
- [12] Martin Schrimpf, Jonas Kubilius, Ha Hong, Najib J. Majaj, Rishi Rajalingham, Elias B. Issa, Kohitij Kar, Pouya Bashivan, Jonathan Prescott-Roy, Franziska Geiger, Kailyn Schmidt, Daniel L. K. Yamins, and James J. DiCarlo. Brain-score: Which artificial neural network for object recognition is most brain-like? *bioRxiv preprint*, 2018.
- [13] Santiago A Cadena, George H Denfield, Edgar Y Walker, Leon A Gatys, Andreas S Tolias, Matthias Bethge, and Alexander S Ecker. Deep convolutional models improve predictions of macaque v1 responses to natural images. *PLoS computational biology*, 15(4):e1006897, 2019.
- [14] Stephen Grossberg. Competitive learning: From interactive activation to adaptive resonance. *Cognitive science*, 11(1):23–63, 1987.

- [15] Sergey Bartunov, Adam Santoro, Blake Richards, Luke Marris, Geoffrey E Hinton, and Timothy Lillicrap. Assessing the scalability of biologically-motivated deep learning algorithms and architectures. In *Advances in Neural Information Processing Systems*, pages 9368–9378, 2018.
- [16] Stéphane d’Ascoli, Levent Sagun, Joan Bruna, and Giulio Biroli. Finding the needle in the haystack with convolutions: on the benefits of architectural bias. *arXiv preprint arXiv:1906.06766*, 2019.
- [17] Martin Schrimpf, Jonas Kubilius, Michael J Lee, N Apurva Ratan Murty, Robert Ajemian, and James J DiCarlo. Integrative benchmarking to advance neurally mechanistic models of human intelligence. *Neuron*, 2020.
- [18] Blake A Richards, Timothy P Lillicrap, Philippe Beaudoin, Yoshua Bengio, Rafal Bogacz, Amelia Christensen, Claudia Clopath, Rui Ponte Costa, Archy de Berker, Surya Ganguli, et al. A deep learning framework for neuroscience. *Nature neuroscience*, 22(11):1761–1770, 2019.
- [19] Arild Nøkland. Direct feedback alignment provides learning in deep neural networks. In *Advances in neural information processing systems*, pages 1037–1045, 2016.
- [20] Theodore H Moskovitz, Ashok Litwin-Kumar, and LF Abbott. Feedback alignment in deep convolutional networks. *arXiv preprint arXiv:1812.06488*, 2018.
- [21] Hesham Mostafa, Vishwajith Ramesh, and Gert Cauwenberghs. Deep supervised learning using local errors. *Frontiers in neuroscience*, 12:608, 2018.
- [22] Arild Nøkland and Lars Hiller Eidnes. Training neural networks with local error signals. *arXiv preprint arXiv:1901.06656*, 2019.
- [23] Mohamed Akrouf, Collin Wilson, Peter Humphreys, Timothy Lillicrap, and Douglas B Tweed. Deep learning without weight transport. In *Advances in Neural Information Processing Systems*, pages 974–982, 2019.
- [24] Axel Laborieux, Maxence Ernoult, Benjamin Scellier, Yoshua Bengio, Julie Grollier, and Damien Querlioz. Scaling equilibrium propagation to deep convnets by drastically reducing its gradient estimator bias. *arXiv preprint arXiv:2006.03824*, 2020.
- [25] Roman Pogodin and Peter E Latham. Kernelized information bottleneck leads to biologically plausible 3-factor hebbian learning in deep networks. *arXiv preprint arXiv:2006.07123*, 2020.
- [26] Behnam Neyshabur. Towards learning convolutions from scratch. *arXiv preprint arXiv:2007.13657*, 2020.
- [27] Gamaleldin Elsayed, Prajit Ramachandran, Jonathon Shlens, and Simon Kornblith. Revisiting spatial invariance with low-rank local connectivity. In Hal Daumé III and Aarti Singh, editors, *Proceedings of the 37th International Conference on Machine Learning*, volume 119 of *Proceedings of Machine Learning Research*, pages 2868–2879. PMLR, 13–18 Jul 2020.
- [28] Alexey Dosovitskiy, Lucas Beyer, Alexander Kolesnikov, Dirk Weissenborn, Xiaohua Zhai, Thomas Unterthiner, Mostafa Dehghani, Matthias Minderer, Georg Heigold, Sylvain Gelly, et al. An image is worth 16x16 words: Transformers for image recognition at scale. *arXiv preprint arXiv:2010.11929*, 2020.
- [29] Nicolas Carion, Francisco Massa, Gabriel Synnaeve, Nicolas Usunier, Alexander Kirillov, and Sergey Zagoruyko. End-to-end object detection with transformers. In *European Conference on Computer Vision*, pages 213–229. Springer, 2020.
- [30] Hugo Touvron, Matthieu Cord, Matthijs Douze, Francisco Massa, Alexandre Sablayrolles, and Hervé Jégou. Training data-efficient image transformers & distillation through attention. *arXiv preprint arXiv:2012.12877*, 2020.
- [31] Xizhou Zhu, Weijie Su, Lewei Lu, Bin Li, Xiaogang Wang, and Jifeng Dai. Deformable detr: Deformable transformers for end-to-end object detection. *arXiv preprint arXiv:2010.04159*, 2020.
- [32] Ilya Tolstikhin, Neil Houlsby, Alexander Kolesnikov, Lucas Beyer, Xiaohua Zhai, Thomas Unterthiner, Jessica Yung, Daniel Keysers, Jakob Uszkoreit, Mario Lucic, and Alexey Dosovitskiy. Mlp-mixer: An all-mlp architecture for vision, 2021.
- [33] Hugo Touvron, Piotr Bojanowski, Mathilde Caron, Matthieu Cord, Alaaeldin El-Nouby, Edouard Grave, Armand Joulin, Gabriel Synnaeve, Jakob Verbeek, and Hervé Jégou. Resmlp: Feedforward networks for image classification with data-efficient training. *arXiv preprint arXiv:2105.03404*, 2021.

- [34] Hanxiao Liu, Zihang Dai, David R So, and Quoc V Le. Pay attention to mlps. *arXiv preprint arXiv:2105.08050*, 2021.
- [35] Alex Krizhevsky, Geoffrey Hinton, et al. Learning multiple layers of features from tiny images. 2009.
- [36] Ya Le and Xuan Yang. Tiny imagenet visual recognition challenge. *CS 231N*, 7:7, 2015.
- [37] Jia Deng, Wei Dong, Richard Socher, Li-Jia Li, Kai Li, and Li Fei-Fei. Imagenet: A large-scale hierarchical image database. In *2009 IEEE conference on computer vision and pattern recognition*, pages 248–255. Ieee, 2009.
- [38] Ilya Loshchilov and Frank Hutter. Decoupled weight decay regularization. *arXiv preprint arXiv:1711.05101*, 2017.
- [39] Adam Paszke, Sam Gross, Francisco Massa, Adam Lerer, James Bradbury, Gregory Chanan, Trevor Killeen, Zeming Lin, Natalia Gimelshein, Luca Antiga, Alban Desmaison, Andreas Kopf, Edward Yang, Zachary DeVito, Martin Raison, Alykhan Tejani, Sasank Chilamkurthy, Benoit Steiner, Lu Fang, Junjie Bai, and Soumith Chintala. Pytorch: An imperative style, high-performance deep learning library. In H. Wallach, H. Larochelle, A. Beygelzimer, F. d'Alché-Buc, E. Fox, and R. Garnett, editors, *Advances in Neural Information Processing Systems 32*, pages 8024–8035. Curran Associates, Inc., 2019.
- [40] Jordan Ott, Erik J. Linstead, Nicholas LaHaye, and Pierre Baldi. Learning in the machine: To share or not to share? *Neural networks : the official journal of the International Neural Network Society*, 126:235–249, 2020.
- [41] Jeremy Freeman, Corey M. Ziemba, David J. Heeger, Eero P. Simoncelli, and J. Anthony Movshon. A functional and perceptual signature of the second visual area in primates. *Nature Neuroscience*, 16(7):974–981, Jul 2013.
- [42] Tiago Marques, Martin Schrimpf, and James J DiCarlo. Multi-scale hierarchical neural network models that bridge from single neurons in the primate primary visual cortex to object recognition behavior. *bioRxiv*, 2021.
- [43] Najib J. Majaj, Ha Hong, Ethan A. Solomon, and James J. DiCarlo. Simple learned weighted sums of inferior temporal neuronal firing rates accurately predict human core object recognition performance. *Journal of Neuroscience*, 35(39):13402–13418, 2015.
- [44] Rishi Rajalingham, Elias B. Issa, Pouya Bashivan, Kohitij Kar, Kailyn Schmidt, and James J. DiCarlo. Large-scale, high-resolution comparison of the core visual object recognition behavior of humans, monkeys, and state-of-the-art deep artificial neural networks. *bioRxiv*, 2018.
- [45] Maximilian Riesenhuber and Tomaso A. Poggio. Hierarchical models of object recognition in cortex. *Nature Neuroscience*, 2:1019–1025, 1999.
- [46] Peter Földiák. Learning invariance from transformation sequences. *Neural computation*, 3(2):194–200, 1991.
- [47] Guy Wallis, Edmund Rolls, and Peter Foldiak. Learning invariant responses to the natural transformations of objects. In *Proceedings of 1993 International Conference on Neural Networks (IJCNN-93-Nagoya, Japan)*, volume 2, pages 1087–1090. IEEE, 1993.
- [48] Laurenz Wiskott and Terrence J Sejnowski. Slow feature analysis: Unsupervised learning of invariances. *Neural computation*, 14(4):715–770, 2002.
- [49] Sushil K Jha, Brian E. Jones, Tammi Coleman, Nick Steinmetz, Chi-Tat Law, Gerald D. Griffin, Joshua D. Hawk, Nooreen Dabbish, Valery A. Kalatsky, and Marcos G. Frank. Sleep-dependent plasticity requires cortical activity. *The Journal of Neuroscience*, 25:9266 – 9274, 2005.
- [50] Carlos Puentes-Mestril and Sara J Aton. Linking network activity to synaptic plasticity during sleep: hypotheses and recent data. *Frontiers in neural circuits*, 11:61, 2017.
- [51] William H. Bosking, Ying Zhang, Brett Schofield, and David Fitzpatrick. Orientation selectivity and the arrangement of horizontal connections in tree shrew striate cortex. *J. Neurosci.*, 15, 1997.
- [52] Robert Mansel Gower, Nicolas Loizou, Xun Qian, Alibek Sailanbayev, Egor Shulgin, and Peter Richtárik. Sgd: General analysis and improved rates. In *International Conference on Machine Learning*, pages 5200–5209. PMLR, 2019.
- [53] Kaiming He, Xiangyu Zhang, Shaoqing Ren, and Jian Sun. Delving deep into rectifiers: Surpassing human-level performance on imagenet classification. In *Proceedings of the IEEE international conference on computer vision*, pages 1026–1034, 2015.

Checklist

1. For all authors...
 - (a) Do the main claims made in the abstract and introduction accurately reflect the paper's contributions and scope? [Yes]
 - (b) Did you describe the limitations of your work? [Yes] See Section 6.
 - (c) Did you discuss any potential negative societal impacts of your work? [Yes] See Section 6.
 - (d) Have you read the ethics review guidelines and ensured that your paper conforms to them? [Yes]
2. If you are including theoretical results...
 - (a) Did you state the full set of assumptions of all theoretical results? [Yes] See the supplementary material.
 - (b) Did you include complete proofs of all theoretical results? [Yes] See the supplementary material.
3. If you ran experiments...
 - (a) Did you include the code, data, and instructions needed to reproduce the main experimental results (either in the supplemental material or as a URL)? [Yes] See <https://github.com/romanpogodin/towards-bio-plausible-conv> and the supplementary material.
 - (b) Did you specify all the training details (e.g., data splits, hyperparameters, how they were chosen)? [Yes] See the supplementary material.
 - (c) Did you report error bars (e.g., with respect to the random seed after running experiments multiple times)? [Yes] See the supplementary material for small-scale experiments. [No] The large-scale experiments were run 1 time due to resource constraints.
 - (d) Did you include the total amount of compute and the type of resources used (e.g., type of GPUs, internal cluster, or cloud provider)? [Yes] See Section 5.
4. If you are using existing assets (e.g., code, data, models) or curating/releasing new assets...
 - (a) If your work uses existing assets, did you cite the creators? [Yes]
 - (b) Did you mention the license of the assets? [No] We used publicly available datasets and open-source repositories.
 - (c) Did you include any new assets either in the supplemental material or as a URL? [Yes] Implementation: <https://github.com/romanpogodin/towards-bio-plausible-conv>
 - (d) Did you discuss whether and how consent was obtained from people whose data you're using/curating? [No] We used publicly available datasets.
 - (e) Did you discuss whether the data you are using/curating contains personally identifiable information or offensive content? [No] We used publicly available datasets.
5. If you used crowdsourcing or conducted research with human subjects...
 - (a) Did you include the full text of instructions given to participants and screenshots, if applicable? [N/A]
 - (b) Did you describe any potential participant risks, with links to Institutional Review Board (IRB) approvals, if applicable? [N/A]
 - (c) Did you include the estimated hourly wage paid to participants and the total amount spent on participant compensation? [N/A]

Appendices

A Dynamic weight sharing

A.1 Noiseless case

Each neuron receives the same k -dimensional input \mathbf{x} , and its response z_i is given by

$$z_i = \mathbf{w}_i^\top \mathbf{x} = \sum_{j=1}^k w_{ij} x_j. \quad (10)$$

To equalize the weights \mathbf{w}_i among all neurons, the network minimizes the following objective,

$$\mathcal{L}_{\text{w. sh.}}(\mathbf{w}_1, \dots, \mathbf{w}_N) = \frac{1}{4MN} \sum_{m=1}^M \sum_{i=1}^N \sum_{j=1}^N (z_i - z_j)^2 + \frac{\gamma}{2} \sum_{i=1}^N \|\mathbf{w}_i - \mathbf{w}_i^{\text{init}}\|^2 \quad (11)$$

$$= \frac{1}{4MN} \sum_{m=1}^M \sum_{i=1}^N \sum_{j=1}^N (\mathbf{w}_i^\top \mathbf{x}_m - \mathbf{w}_j^\top \mathbf{x}_m)^2 + \frac{\gamma}{2} \sum_{i=1}^N \|\mathbf{w}_i - \mathbf{w}_i^{\text{init}}\|^2, \quad (12)$$

where $\mathbf{w}_i^{\text{init}}$ is the weight at the start of dynamic weight sharing. This is a strongly convex function, and therefore it has a unique minimum.

The SGD update for one \mathbf{x}_m is

$$\Delta \mathbf{w}_i \propto - \left(z_i - \frac{1}{N} \sum_{j=1}^N z_j \right) \mathbf{x}_m - \gamma (\mathbf{w}_i - \mathbf{w}_i^{\text{init}}). \quad (13)$$

To find the fixed point of the dynamics, we first set the sum over the gradients to zero,

$$\sum_i \frac{d \mathcal{L}_{\text{w. sh.}}(\mathbf{w}_1, \dots, \mathbf{w}_N)}{d \mathbf{w}_i} = \frac{1}{M} \sum_{i,m} \left(z_i - \frac{1}{N} \sum_{j=1}^N z_j \right) \mathbf{x}_m + \gamma \sum_i (\mathbf{w}_i - \mathbf{w}_i^{\text{init}}) \quad (14)$$

$$= \gamma \sum_i (\mathbf{w}_i - \mathbf{w}_i^{\text{init}}) = 0. \quad (15)$$

Therefore, at the fixed point the mean weight $\boldsymbol{\mu}^* = \sum_i \mathbf{w}_i^*/N$ is equal to $\boldsymbol{\mu}^{\text{init}} = \sum_i \mathbf{w}_i^{\text{init}}/N$, and

$$\frac{1}{N} \sum_{i=1}^N z_i = \frac{1}{N} \sum_{i=1}^N \mathbf{w}_i^{*\top} \mathbf{x}_m = (\boldsymbol{\mu}^{\text{init}})^\top \mathbf{x}_m. \quad (16)$$

We can now find the individual weights,

$$\frac{d \mathcal{L}_{\text{w. sh.}}(\mathbf{w}_1, \dots, \mathbf{w}_N)}{d \mathbf{w}_i} = \frac{1}{M} \sum_m \left(z_i - \frac{1}{N} \sum_{j=1}^N z_j \right) \mathbf{x}_m + \gamma (\mathbf{w}_i - \mathbf{w}_i^{\text{init}}) \quad (17)$$

$$= \frac{1}{M} \sum_m \mathbf{x}_m \mathbf{x}_m^\top (\mathbf{w}_i - \boldsymbol{\mu}^{\text{init}}) + \gamma (\mathbf{w}_i - \mathbf{w}_i^{\text{init}}) = 0. \quad (18)$$

Denoting the covariance matrix $\mathbf{C} \equiv \frac{1}{M} \sum_m \mathbf{x}_m \mathbf{x}_m^\top$, we see that

$$\mathbf{w}_i^* = (\mathbf{C} + \gamma \mathbf{I})^{-1} (\mathbf{C} \boldsymbol{\mu}^{\text{init}} + \gamma \mathbf{w}_i^{\text{init}}) = (\mathbf{C} + \gamma \mathbf{I})^{-1} \left(\mathbf{C} \frac{1}{N} \sum_{i=1}^N \mathbf{w}_i^{\text{init}} + \gamma \mathbf{w}_i^{\text{init}} \right), \quad (19)$$

where \mathbf{I} is the identity matrix. From Eq. (19) it is clear that $\mathbf{w}_i^* \approx \boldsymbol{\mu}^{\text{init}}$ for small γ and full rank \mathbf{C} . For instance, for $\mathbf{C} = \mathbf{I}$,

$$\mathbf{w}_i^* = \frac{1}{1 + \gamma} \boldsymbol{\mu}^{\text{init}} + \frac{\gamma}{1 + \gamma} \mathbf{w}_i^{\text{init}}. \quad (20)$$

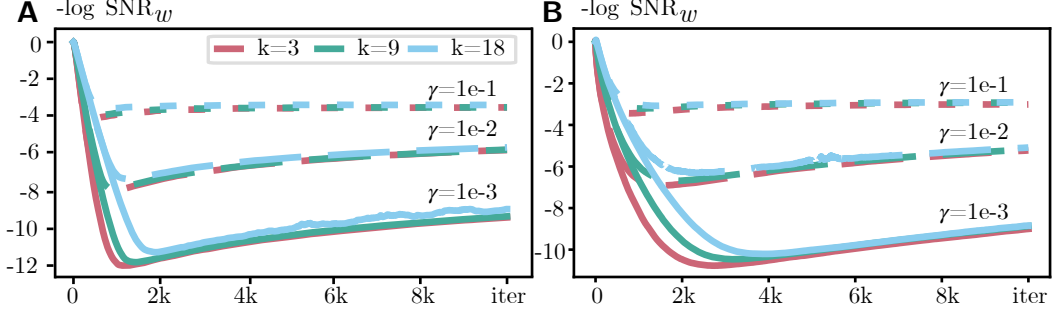


Figure 5: Logarithm of inverse signal-to-noise ratio (mean weight squared over weight variance, see Eq. (6)) for weight sharing objectives in a layer with 100 neurons. **A.** Dynamics of Eq. (21) for different kernel sizes k (meaning k^2 inputs) and γ . **B.** Dynamics of weight update that uses Eq. (8b) for $\alpha = 10$, different kernel sizes k and γ . In each iteration, the input is presented for 150 ms.

A.2 Biased noiseless case, and its correspondence to the realistic implementation

The realistic implementation of dynamic weight sharing with an inhibitory neuron (Section 4.2) introduces a bias in the update rule: Eq. (13) becomes

$$\Delta \mathbf{w}_i \propto - \left(z_i - \frac{\alpha}{N(1+\alpha)} \sum_{j=1}^N z_j \right) \mathbf{x}_m - \gamma (\mathbf{w}_i - \mathbf{w}_i^{\text{init}}) \quad (21)$$

for inhibition strength α .

Following the same derivation as for the unbiased case, we can show that the weight dynamics converges to

$$\sum_i \frac{d \mathcal{L}_{\text{w. sh.}}(\mathbf{w}_1, \dots, \mathbf{w}_N)}{d \mathbf{w}_i} = \frac{1}{M} \sum_{i,m} \left(z_i - \frac{\alpha}{1+\alpha} \frac{1}{N} \sum_{j=1}^N z_j \right) \mathbf{x}_m + \gamma \sum_i (\mathbf{w}_i - \mathbf{w}_i^{\text{init}}) \quad (22)$$

$$= \frac{1}{1+\alpha} \mathbf{C} \sum_i \mathbf{w}_i + \gamma \sum_i (\mathbf{w}_i - \mathbf{w}_i^{\text{init}}) = 0. \quad (23)$$

Therefore $\boldsymbol{\mu}^* = \gamma \left(\frac{1}{1+\alpha} \mathbf{C} + \gamma \mathbf{I} \right)^{-1} \boldsymbol{\mu}^{\text{init}}$, and

$$\mathbf{w}_i^* = (\mathbf{C} + \gamma \mathbf{I})^{-1} \left(\frac{\gamma \alpha}{1+\alpha} \mathbf{C} \left(\frac{1}{1+\alpha} \mathbf{C} + \gamma \mathbf{I} \right)^{-1} \boldsymbol{\mu}^{\text{init}} + \gamma \mathbf{w}_i^{\text{init}} \right). \quad (24)$$

For $\mathbf{C} = \mathbf{I}$, this becomes

$$\mathbf{w}_i^* = \frac{\gamma}{1+\gamma} \left(\frac{\alpha}{1+\gamma(1+\alpha)} \boldsymbol{\mu}^{\text{init}} + \mathbf{w}_i^{\text{init}} \right). \quad (25)$$

As a result, the final weights are approximately the same among neurons, but have a small norm due to the γ scaling.

The dynamics in Eq. (21) correctly captures the bias influence in Eq. (8b), producing similar SNR plots; compare Fig. 5A (Eq. (21) dynamics) to Fig. 5B (Eq. (8b) dynamics). The curves are slightly different due to different learning rates, but both follow the same trend of first finding a very good solution, and then slowly incorporating the bias term (leading to smaller SNR).

A.3 Noisy case

Realistically, all neurons can't see the same \mathbf{x}_m . However, due to the properties of our loss, we can work even with noisy updates. To see this, we write the objective function as

$$\mathcal{L}_{\text{w. sh.}}(\mathbf{w}_1, \dots, \mathbf{w}_N) = \frac{1}{M} \sum_{m=1}^M f(\mathbf{W}, \mathbf{X}_m) \quad (26)$$

where matrices \mathbf{W} and \mathbf{X} satisfy $(\mathbf{W})_i = \mathbf{w}_i$ and $(\mathbf{X}_m)_i = \mathbf{x}_m$, and

$$f(\mathbf{W}, \mathbf{X}_m) = \frac{1}{4N} \sum_{i=1}^N \sum_{j=1}^N (\mathbf{w}_i^\top \mathbf{x}_m - \mathbf{w}_j^\top \mathbf{x}_m)^2 + \frac{\gamma}{2} \sum_{i=1}^N \|\mathbf{w}_i - \mathbf{w}_i^{\text{init}}\|^2. \quad (27)$$

We'll update the weights with SGD according to

$$\Delta \mathbf{W}^{k+1} = -\eta_k \left. \frac{d}{d\mathbf{W}} f(\mathbf{W}, \mathbf{X}_{m(k)} + \mathbf{E}^k) \right|_{\mathbf{W}^k}, \quad (28)$$

where $(\mathbf{E}^k)_i = \epsilon_i$ is zero-mean input noise and $m(k)$ is chosen uniformly.

Let's also bound the input mean and noise as

$$\mathbb{E}_{\mathbf{E}} \|\mathbf{x}_{m(k)} + \epsilon_i\|^2 \leq \sqrt{c_{x\epsilon}}, \quad \mathbb{E}_{\mathbf{E}} \|\mathbf{x}_{m(k)} + \epsilon_i\|^4 \leq c_{x\epsilon}. \quad (29)$$

With this setup, we can show that SGD with noise can quickly converge to the correct solution, apart from a constant noise-induced bias. Our analysis is standard and follows [52], but had to be adapted for our objective and noise model.

Theorem 1. *For zero-mean isotropic noise \mathbf{E} with variance σ^2 , uniform SGD sampling $m(k)$ and inputs \mathbf{x}_m that satisfy Eq. (29), choosing $\eta_k = O(1/k)$ leads to*

$$\mathbb{E} \|\mathbf{W}^{k+1} - \mathbf{W}^*\|_F^2 = O\left(\frac{\|\mathbf{W}^{\text{init}} - \mathbf{W}^*\|_F}{k+1}\right) + O(\sigma^2 \|\mathbf{W}^*\|_F^2), \quad (30)$$

where $(\mathbf{W}^*)_i$ is given by Eq. (19).

Proof. Using the SGD update,

$$\|\mathbf{W}^{k+1} - \mathbf{W}^*\|_F^2 = \left\| \mathbf{W}^k - \eta_k \left. \frac{d}{d\mathbf{W}} f(\mathbf{W}, \mathbf{X}_{m(k)} + \mathbf{E}^k) \right|_{\mathbf{W}^k} - \mathbf{W}^* \right\|_F^2 \quad (31)$$

$$= \|\mathbf{W}^k - \mathbf{W}^*\|_F^2 - 2\eta_k \left\langle \mathbf{W}^k - \mathbf{W}^*, \left. \frac{d}{d\mathbf{W}} f(\mathbf{W}, \mathbf{X}_{m(k)} + \mathbf{E}^k) \right|_{\mathbf{W}^k} \right\rangle \quad (32)$$

$$+ \eta_k^2 \left\| \left. \frac{d}{d\mathbf{W}} f(\mathbf{W}, \mathbf{X}_{m(k)} + \mathbf{E}^k) \right|_{\mathbf{W}^k} \right\|_F^2. \quad (33)$$

We need to bound the second and the third terms in the equation above.

Second term. As f is γ -strongly convex in \mathbf{W} ,

$$- \left\langle \mathbf{W}^k - \mathbf{W}^*, \left. \frac{d}{d\mathbf{W}} f(\mathbf{W}, \mathbf{X}_{m(k)} + \mathbf{E}^k) \right|_{\mathbf{W}^k} \right\rangle \quad (34)$$

$$\leq f(\mathbf{W}^*, \mathbf{X}_{m(k)} + \mathbf{E}^k) - f(\mathbf{W}^k, \mathbf{X}_{m(k)} + \mathbf{E}^k) - \frac{\gamma}{2} \|\mathbf{W}^k - \mathbf{W}^*\|_F^2. \quad (35)$$

As f is convex in \mathbf{X} ,

$$f(\mathbf{W}^*, \mathbf{X}_{m(k)} + \mathbf{E}^k) - f(\mathbf{W}^k, \mathbf{X}_{m(k)} + \mathbf{E}^k) \leq f(\mathbf{W}^*, \mathbf{X}_{m(k)}) - f(\mathbf{W}^k, \mathbf{X}_{m(k)}) \quad (36)$$

$$+ \left\langle \left. \frac{d}{d\mathbf{X}} f(\mathbf{W}^*, \mathbf{X}) \right|_{\mathbf{X}_{m(k)} + \mathbf{E}^k} - \left. \frac{d}{d\mathbf{X}} f(\mathbf{W}^k, \mathbf{X}) \right|_{\mathbf{X}_{m(k)}} , \mathbf{E}^k \right\rangle. \quad (37)$$

We only need to clarify one term here,

$$\left(\frac{d}{d\mathbf{X}} f(\mathbf{W}^*, \mathbf{X}) \Big|_{\mathbf{X}_{m(k)} + \mathbf{E}^k} \right)_i = \left(\frac{d}{d\mathbf{X}} f(\mathbf{W}^*, \mathbf{X}) \Big|_{\mathbf{X}_{m(k)}} \right)_i + \left(\mathbf{w}_i^{*\top} \boldsymbol{\epsilon}_i - \frac{1}{N} \sum_j \mathbf{w}_j^{*\top} \boldsymbol{\epsilon}_j \right) \mathbf{w}_i^*. \quad (38)$$

Now we can take the expectation over $m(k)$ and \mathbf{E} . As $m(k)$ is uniform, and \mathbf{W}^* minimizes the global function,

$$\mathbb{E}_{m(k)} (f(\mathbf{W}^*, \mathbf{X}_{m(k)}) - f(\mathbf{W}^k, \mathbf{X}_{m(k)})) = \mathcal{L}_{\text{w. sh.}}(\mathbf{w}_1^*, \dots, \mathbf{w}_N^*) - \mathcal{L}_{\text{w. sh.}}(\mathbf{w}_1^k, \dots, \mathbf{w}_N^k) \leq 0. \quad (39)$$

As \mathbf{E}^k is zero-mean and isotropic with variance σ^2 ,

$$\mathbb{E}_{m(k), \mathbf{E}^k} \left\langle \frac{d}{d\mathbf{X}} f(\mathbf{W}^*, \mathbf{X}) \Big|_{\mathbf{X}_{m(k)} + \mathbf{E}^k} - \frac{d}{d\mathbf{X}} f(\mathbf{W}^k, \mathbf{X}) \Big|_{\mathbf{X}_{m(k)}}, \mathbf{E}^k \right\rangle \quad (40)$$

$$= \mathbb{E}_{\mathbf{E}^k} \sum_i \left(\mathbf{w}_i^{*\top} \boldsymbol{\epsilon}_i - \frac{1}{N} \sum_j \mathbf{w}_j^{*\top} \boldsymbol{\epsilon}_j \right) \mathbf{w}_i^{*\top} \boldsymbol{\epsilon}_i = \left(1 - \frac{1}{N} \right) \mathbb{E}_{\mathbf{E}^k} \sum_i (\mathbf{w}_i^{*\top} \boldsymbol{\epsilon}_i)^2 \quad (41)$$

$$= \left(1 - \frac{1}{N} \right) \mathbb{E}_{\mathbf{E}^k} \sum_i \text{Tr} (\mathbf{w}_i^* \mathbf{w}_i^{*\top} \boldsymbol{\epsilon}_i \boldsymbol{\epsilon}_i^\top) \leq \sigma^2 \|\mathbf{W}^*\|_F^2. \quad (42)$$

So the whole second term becomes

$$-2\eta_k \mathbb{E}_{m(k), \mathbf{E}} \left\langle \mathbf{W}^k - \mathbf{W}^*, \frac{d}{d\mathbf{W}} f(\mathbf{W}, \mathbf{X}_{m(k)} + \mathbf{E}^k) \Big|_{\mathbf{W}^k} \right\rangle \quad (43)$$

$$\leq -\gamma \eta_k \mathbb{E}_{m(k), \mathbf{E}^k} \|\mathbf{W}^k - \mathbf{W}^*\|_F^2 + \eta_k \sigma^2 \|\mathbf{W}^*\|_F^2. \quad (44)$$

Third term. First, observe that

$$\frac{d}{d\mathbf{w}_i} f(\mathbf{W}, \mathbf{X}) = \mathbf{x}_i \mathbf{x}_i^\top \mathbf{w}_i - \mathbf{x}_i \frac{1}{N} \sum_j \mathbf{x}_j^\top \mathbf{w}_j + \gamma \mathbf{w}_i - \gamma \mathbf{w}_i^{\text{init}} \quad (45)$$

$$= \left(1 - \frac{1}{N} \right) \mathbf{A}_i \mathbf{w}_i - \mathbf{B}_i \mathbf{W} + \gamma \mathbf{w}_i - \gamma \mathbf{w}_i^{\text{init}}, \quad (46)$$

where $\mathbf{A}_i = \mathbf{x}_i \mathbf{x}_i^\top$ and $(\mathbf{B}_i)_j = \mathbb{I}[i \neq j] \mathbf{x}_i \mathbf{x}_j^\top / N$.

Therefore, using $\|a+b\|^2 \leq 2\|a\|^2 + 2\|b\|^2$ twice, properties of the matrix 2-norm, and $(1-1/N) \leq 1$,

$$\left\| \frac{d}{d\mathbf{w}_i} f(\mathbf{W}, \mathbf{X}) \right\|^2 \leq 4 \|\mathbf{A}_i\|_2^2 \|\mathbf{w}_i\|^2 + 4 \|\mathbf{B}_i\|_2^2 \|\mathbf{W}\|^2 + 4\gamma^2 \|\mathbf{w}_i\|^2 + 4\gamma^2 \|\mathbf{w}_i^{\text{init}}\|^2. \quad (47)$$

In our particular case, bounding the 2 norm with the Frobenius norm gives

$$\mathbb{E}_{m(k), \mathbf{E}} \|\mathbf{A}_i\|_2^2 \leq \mathbb{E}_{m(k), \mathbf{E}} \|(\mathbf{x}_{m(k)} + \boldsymbol{\epsilon}_i)(\mathbf{x}_{m(k)} + \boldsymbol{\epsilon}_i)^\top\|_F^2 \quad (48)$$

$$= \mathbb{E}_{m(k), \mathbf{E}} \|\mathbf{x}_{m(k)} + \boldsymbol{\epsilon}_i\|^4 \leq c_{x\epsilon}. \quad (49)$$

Similarly,

$$\mathbb{E}_{m(k), \mathbf{E}} \|\mathbf{B}_i\|_2^2 \leq \mathbb{E}_{m(k), \mathbf{E}} \|\mathbf{B}_i\|_F^2 \leq \frac{1}{N^2} \mathbb{E}_{m(k), \mathbf{E}} \sum_{j \neq i} \|\mathbf{x}_{m(k)} + \boldsymbol{\epsilon}_i\|^2 \|\mathbf{x}_{m(k)} + \boldsymbol{\epsilon}_j\|^2 \leq \frac{c_{x\epsilon}}{N}. \quad (50)$$

Therefore, we can bound the full gradient by the sum of individual bounds (as it's the Frobenius norm) and using $\|a+b\|^2 \leq 2\|a\|^2 + 2\|b\|^2$ again,

$$\mathbb{E}_{m(k), \mathbf{E}} \left\| \frac{d}{d\mathbf{W}} f(\mathbf{W}, \mathbf{X}_{m(k)} + \mathbf{E}^k) \Big|_{\mathbf{W}^k} \right\|_F^2 \leq 4(2c_{x\epsilon} + \gamma^2) \|\mathbf{W}^k\|_F^2 + 4\gamma^2 \|\mathbf{W}^{\text{init}}\|_F^2 \quad (51)$$

$$\leq 8(2c_{x\epsilon} + \gamma^2) \|\mathbf{W}^k - \mathbf{W}^*\|_F^2 + 8(2c_{x\epsilon} + \gamma^2) \|\mathbf{W}^*\|_F^2 + 4\gamma^2 \|\mathbf{W}^{\text{init}}\|_F^2. \quad (52)$$

Combining all of this, and taking the expectation over all steps before $k + 1$, gives us

$$\mathbb{E} \|\mathbf{W}^{k+1} - \mathbf{W}^*\|_F^2 \leq (1 - \gamma\eta_k + \eta_k^2 8(2c_{x\epsilon} + \gamma^2)) \mathbb{E} \|\mathbf{W}^k - \mathbf{W}^*\|_F^2 \quad (53)$$

$$+ \eta_k \sigma^2 \|\mathbf{W}^*\|_F^2 + \eta_k^2 \left(8(2c_{x\epsilon} + \gamma^2) \|\mathbf{W}^*\|_F^2 + 4\gamma^2 \|\mathbf{W}^{\text{init}}\|_F^2 \right). \quad (54)$$

If we choose η_k such that $\eta_k \cdot \left(8(2c_{x\epsilon} + \gamma^2) \|\mathbf{W}^*\|_F^2 + 4\gamma^2 \|\mathbf{W}^{\text{init}}\|_F^2 \right) \leq \sigma^2$, we can simplify the result,

$$\mathbb{E} \|\mathbf{W}^{k+1} - \mathbf{W}^*\|_F^2 \leq (1 - \gamma\eta_k + \eta_k^2 8(2c_{x\epsilon} + \gamma^2)) \mathbb{E} \|\mathbf{W}^k - \mathbf{W}^*\|_F^2 + 2\eta_k \sigma^2 \|\mathbf{W}^*\|_F^2 \quad (55)$$

$$\leq \left(\prod_{s=0}^k (1 - \gamma\eta_s + \eta_s^2 8(2c_{x\epsilon} + \gamma^2)) \right) \mathbb{E} \|\mathbf{W}^{\text{init}} - \mathbf{W}^*\|_F^2 \quad (56)$$

$$+ 2\sigma^2 \sum_{t=0}^k \eta_t \left(\prod_{s=1}^t (1 - \gamma\eta_s + \eta_s^2 8(2c_{x\epsilon} + \gamma^2)) \right) \|\mathbf{W}^*\|_F^2. \quad (57)$$

If we choose $\eta_k = O(1/k)$, the first term will decrease as $1/k$. The second one will stay constant with time, and proportional to σ^2 .

□

A.4 Applicability to vision transformers

In vision transformers (e.g. [28]), an input image is reshaped into a matrix $\mathbf{Z} \in \mathbb{R}^{N \times D}$ for N non-overlapping patches of the input, each of size D . As the first step, \mathbf{Z} is multiplied by a matrix $\mathbf{U} \in \mathbb{R}^{D \times 3D}$ as $\mathbf{Z}' = \mathbf{Z}\mathbf{U}$. Therefore, an output neuron $z'_{i,j} = \sum_k z_{ik} u_{kj}$ looks at \mathbf{z}_i with the same weights as $z'_{i',j} = \sum_k z_{i'k} u_{kj}$ uses for $\mathbf{z}_{i'}$ for any i' .

To share weights with dynamic weight sharing, for each k we need to connect all z_{ik} across i (input layer), and for each j – all $z'_{i,j}$ across i (output layer). After that, weight sharing will proceed just like for locally connected networks: activate an input grid j_1 (one of D possible ones) to create a repeating input patten, then activate a grid j_2 and so on.

A.5 Details for convergence plots

Both plots in Fig. 4 show mean negative log SNR over 10 runs, 100 output neurons each. Initial weights were drawn from $\mathcal{N}(1, 1)$. At every iteration, the new input \mathbf{x} was drawn from $\mathcal{N}(1, 1)$ independently for each component. Learning was performed via SGD with momentum of 0.95. The minimum SNR value was computed from Eq. (5). For our data, the SNR expression in Eq. (6) has $\left(\frac{1}{N} \sum_i (\mathbf{w}_i)_j \right)^2 \approx 1$ and $\frac{1}{N} \sum_i \left((\mathbf{w}_i)_j - \frac{1}{N} \sum_{i'} (\mathbf{w}_{i'})_j \right)^2 \approx \gamma^2 / (1 + \gamma)^2$, therefore $-\log \text{SNR}_{\min} = 2 \log(\gamma / (1 + \gamma))$.

For Fig. 4A, we performed 2000 iterations (with a new \mathbf{x} each time). Learning rate at iteration k was $\eta_k = 0.5 / (1000 + k)$. For Fig. 5A, we did the same simulation but for 10^4 iterations.

For Fig. 4B, network dynamics (Eq. (8b)) was simulated with $\tau = 30$ ms, $b = 1$ using Euler method with steps size of 1 ms. We performed 10^4 iterations (150 ms per iteration, with a new \mathbf{x} each iteration). Learning rate at iteration k was $\eta_k = 0.0003 / \sqrt{1 + k/2} \cdot \mathbb{I}[k \geq 50]$.

The code for both runs is provided in the supplementary material.

B Experimental details

Both convolutional and LC layers did not have the bias term, and were initialized according to Kaiming Normal initialization [53] with ReLU gain, meaning each weight was drawn from $\mathcal{N}(0, 2 / (c_{\text{out}} k^2))$ for kernel size k and c_{out} output channels.

All runs were done with automatic mixed precision, meaning that inputs to each layer (but not the weights) were stored as float16, and not float32. This greatly improved performance and memory requirements of the networks.

As an aside, the weight dynamics of sleep/training phases indeed followed Fig. 3A. Fig. 6 shows $-\log \text{SNR}_w$ (defined in Eq. (6)) for weight sharing every 10 iterations on CIFAR10. For small learning rates, the weights do not diverge too much in-between sleep phases.

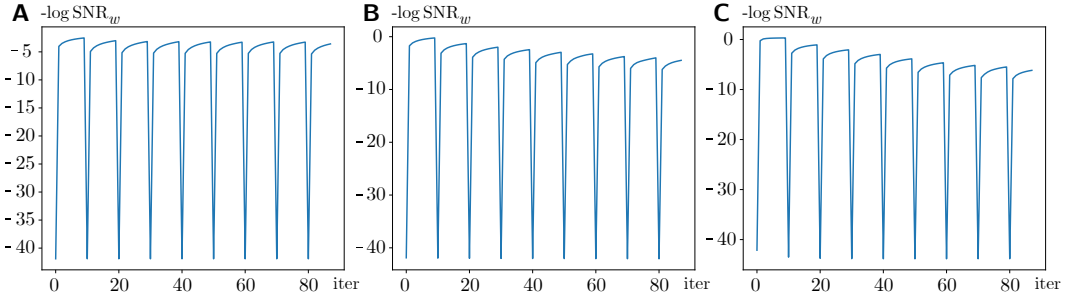


Figure 6: Logarithm of inverse signal-to-noise ratio (mean weight squared over weight variance, see Eq. (6)) for weight sharing every 10 iterations for CIFAR10. **A.** Learning rate = $5e-4$. **B.** Learning rate = $5e-3$. **C.** Learning rate = $5e-2$.

B.1 CIFAR10/100, TinyImageNet

Mean performance over 5 runs is summarized in Table 4 (padding of 0), Table 5 (padding of 4), and Table 6 (padding of 8). Maximum minus minimum accuracy is summarized in Table 7, Table 8, and Table 9. Hyperparameters for AdamW (learning rate and weight decay) are provided in Table 10, Table 11, and Table 12.

Hyperparameters were optimized on a train/validation split (see Section 5) over the following grids. **CIFAR10/100.** Learning rate: [$1e-1$, $5e-2$, $1e-2$, $5e-3$] (conv), [$1e-3$, $5e-4$, $1e-4$, $5e-5$] (LC); weight decay [$1e-2$, $1e-4$] (both). **TinyImageNet.** Learning rate: [$5e-3$, $1e-3$, $5e-4$] (conv), [$1e-3$, $5e-4$] (LC); weight decay [$1e-2$, $1e-4$] (both). The learning rate range for TinyImageNet was smaller as preliminary experiments showed poor performance for slow learning rates.

For all runs, the batch size was 512. For all final runs, learning rate was divided by 4 at 100 and then at 150 epochs (out of 200). Grid search for CIFAR10/100 was done for the same 200 epochs setup. For TinyImageNet, grid search was performed over 50 epochs with learning rate decreases at 25 and 37 epochs (i.e., the same schedule but compressed) due to the larger computational cost of full runs.

B.2 ImageNet

In addition to the main results, we also tested the variant of the locally connected network with a convolutional first layer (Table 13). It improved performance for all configurations: from about 2% for weight sharing every 1-10 iterations, to about 5% for 100 iterations and for no weight sharing. This is not surprising, as the first layer has the largest resolution (224 by 224; initially, we performed these experiment due to memory constraints). Our result suggests that adding a “good” pre-processing layer (e.g. the retina) can also improve performance of locally connected networks.

Final hyperparameters. Learning rate: $1e-3$ (conv, LC with w.sh. (1)), $5e-4$ (all other LC; all LC with 1st layer conv), weight decay: $1e-2$ (all). Hyperparameters were optimized on a train/validation split (see Section 5) over the following grids. Conv: learning rate [$1e-3$, $5e-4$], weight decay [$1e-2$, $1e-4$, $1e-6$]. LC: learning rate [$1e-3$, $5e-4$, $1e-4$, $5e-5$], weight decay [$1e-2$]. LC (1st layer conv): learning rate [$1e-3$, $5e-4$], weight decay [$1e-2$, $1e-4$, $1e-6$]. For LC, we only tried the large weight decay based on earlier experiment (LC (1st layer conv)). For LC (1st layer conv), we only tuned hyperparameters for LC and LC with weight sharing in each iteration, as they found the same values (weight sharing every 10/100 iterations interpolates between LC and LC with weight sharing in each iteration, and therefore is expected to behave similarly to both). In addition, for LC (1st layer conv) we only tested learning rate of $5e-4$ for weight decay of $1e-2$ as higher learning rates performed significantly worse for other runs (and in preliminary experiments).

For all runs, the batch size was 256. For all final runs, learning rate was divided by 4 at 100 and then at 150 epochs (out of 200). Grid search was performed over 20 epochs with learning rate decreases at

Table 4: Performance of convolutional (conv) and locally connected (LC) networks for padding of 0 in the input images (mean accuracy over 5 runs). For LC, two regularization strategies were applied: repeating the same image n times with different translations (n reps) or using dynamic weight sharing every n batches (ws (n)). LC nets additionally show performance difference w.r.t. conv nets.

Regularizer	Connectivity	CIFAR10		CIFAR100				TinyImageNet			
		Top-1 accuracy (%)	Diff	Top-1 accuracy (%)	Diff	Top-5 accuracy (%)	Diff	Top-1 accuracy (%)	Diff	Top-5 accuracy (%)	Diff
-	conv	84.1	-	49.5	-	78.2	-	26.0	-	51.2	-
	LC	67.2	-16.8	34.9	-14.6	62.2	-16.0	12.0	-14.1	30.4	-20.7
Weight Sharing	LC - ws(1)	74.8	-9.3	41.8	-7.7	70.1	-8.1	24.9	-1.2	49.1	-2.1
	LC - ws(10)	75.9	-8.1	44.4	-5.1	72.0	-6.2	28.1	2.0	52.5	1.3
	LC - ws(100)	75.4	-8.6	43.4	-6.1	71.9	-6.3	27.4	1.3	51.9	0.8

Table 5: Mean performance over 5 runs. Same as Table 4, but for padding of 4.

Regularizer	Connectivity	CIFAR10		CIFAR100				TinyImageNet			
		Top-1 accuracy (%)	Diff	Top-1 accuracy (%)	Diff	Top-5 accuracy (%)	Diff	Top-1 accuracy (%)	Diff	Top-5 accuracy (%)	Diff
-	conv	88.3	-	59.2	-	84.9	-	38.6	-	65.1	-
	LC	80.9	-7.4	49.8	-9.4	75.5	-9.4	29.6	-9.0	52.7	-12.4
Data Translation	LC - 4 reps	82.9	-5.4	52.1	-7.1	76.4	-8.5	31.9	-6.7	54.9	-10.2
	LC - 8 reps	83.8	-4.5	54.3	-5.0	77.9	-7.0	33.0	-5.6	55.6	-9.5
	LC - 16 reps	85.0	-3.3	55.9	-3.3	78.8	-6.1	34.0	-4.6	56.2	-8.8
Weight Sharing	LC - ws(1)	87.4	-0.8	58.7	-0.5	83.4	-1.6	41.6	3.0	66.1	1.1
	LC - ws(10)	85.1	-3.2	55.7	-3.6	80.9	-4.0	37.4	-1.2	61.8	-3.2
	LC - ws(100)	82.0	-6.3	52.8	-6.4	80.1	-4.8	37.1	-1.5	62.8	-2.3

10 and 15 epochs (i.e., the same schedule but compressed) due to the large computational cost of full runs.

Table 6: Mean performance over 5 runs. Same as Table 4, but for padding of 8.

Regularizer	Connectivity	CIFAR10		CIFAR100				TinyImageNet			
		Top-1 accuracy (%)	Diff	Top-1 accuracy (%)	Diff	Top-5 accuracy (%)	Diff	Top-1 accuracy (%)	Diff	Top-5 accuracy (%)	Diff
-	conv	88.7	-	59.6	-	85.4	-	42.6	-	68.7	-
	LC	80.7	-8.0	47.7	-11.8	74.8	-10.6	31.9	-10.7	55.4	-13.3
Data Translation	LC - 4 reps	82.8	-6.0	50.6	-9.0	76.2	-9.2	35.5	-7.1	58.6	-10.1
	LC - 8 reps	83.6	-5.1	53.0	-6.6	77.4	-8.0	35.8	-6.7	59.0	-9.7
	LC - 16 reps	85.0	-3.8	55.6	-4.0	78.4	-7.0	37.9	-4.7	60.3	-8.4
Weight Sharing	LC - ws(1)	87.8	-0.9	59.2	-0.4	84.0	-1.4	43.6	1.0	67.9	-0.9
	LC - ws(10)	84.3	-4.5	53.7	-5.8	80.4	-5.0	39.6	-2.9	64.5	-4.3
	LC - ws(100)	79.5	-9.3	50.0	-9.6	78.6	-6.8	39.2	-3.4	64.8	-3.9

Table 7: Max minus min performance over 5 runs; padding of 0.

Regularizer	Connectivity	CIFAR10		CIFAR100		TinyImageNet	
		Top-1 accuracy (%)	Top-1 accuracy (%)	Top-5 accuracy (%)	Top-1 accuracy (%)	Top-5 accuracy (%)	
-	conv	0.5	1.0	1.7	1.0	0.4	
	LC	0.4	1.6	1.5	1.0	1.7	
Weight Sharing	LC - ws(1)	0.5	1.3	1.3	1.2	2.0	
	LC - ws(10)	0.8	1.0	0.7	1.8	2.1	
	LC - ws(100)	0.9	0.7	0.9	1.0	1.3	

Table 8: Max minus min performance over 5 runs; padding of 4.

Regularizer	Connectivity	CIFAR10		CIFAR100		TinyImageNet	
		Top-1 accuracy (%)	Top-1 accuracy (%)	Top-5 accuracy (%)	Top-1 accuracy (%)	Top-5 accuracy (%)	
-	conv	0.7	1.5	0.2	1.2	1.1	
	LC	0.8	1.1	0.4	0.7	0.8	
Data Translation	LC - 4 reps	0.8	1.3	0.8	0.5	0.8	
	LC - 8 reps	0.3	1.4	1.3	0.7	1.2	
	LC - 16 reps	0.7	0.7	0.6	0.9	0.5	
Weight Sharing	LC - ws(1)	0.5	1.1	0.9	0.9	0.6	
	LC - ws(10)	0.6	1.1	0.3	0.6	1.2	
	LC - ws(100)	0.7	1.0	0.6	0.2	0.9	

Table 9: Max minus min performance over 5 runs; padding of 8.

Regularizer	Connectivity	CIFAR10		CIFAR100		TinyImageNet	
		Top-1 accuracy (%)	Top-1 accuracy (%)	Top-5 accuracy (%)	Top-1 accuracy (%)	Top-5 accuracy (%)	
-	conv	0.9	1.5	1.2	1.7	1.0	
	LC	0.5	0.6	0.5	0.5	0.9	
Data Translation	LC - 4 reps	0.4	0.9	0.3	0.6	0.8	
	LC - 8 reps	0.6	0.9	0.5	0.5	0.6	
	LC - 16 reps	0.9	0.9	0.6	0.5	1.1	
Weight Sharing	LC - ws(1)	0.4	1.2	1.5	0.7	0.7	
	LC - ws(10)	0.2	1.4	0.9	1.4	1.2	
	LC - ws(100)	0.4	0.5	0.7	0.7	0.9	

Table 10: Hyperparameters for padding of 0.

Regularizer	Connectivity	CIFAR10		CIFAR100		TinyImageNet	
		Learning rate	Weight decay	Learning rate	Weight decay	Learning rate	Weight decay
-	conv	0.01	0.01	0.01	0.01	0.005	0.01
	LC	0.001	0.01	0.001	0.01	0.001	0.0001
Weight Sharing	LC - ws(1)	0.001	0.01	0.001	0.01	0.001	0.0001
	LC - ws(10)	0.0005	0.01	0.0005	0.0001	0.0005	0.01
	LC - ws(100)	0.0001	0.01	0.0001	0.01	0.001	0.0001

Table 11: Hyperparameters for padding of 4.

Regularizer	Connectivity	CIFAR10		CIFAR100		TinyImageNet	
		Learning rate	Weight decay	Learning rate	Weight decay	Learning rate	Weight decay
-	conv	0.01	0.0001	0.01	0.01	0.005	0.0001
	LC	0.001	0.0001	0.0005	0.01	0.0005	0.0001
Data Translation	LC - 4 reps	0.001	0.01	0.001	0.01	0.0005	0.01
	LC - 8 reps	0.0005	0.01	0.0005	0.0001	0.0005	0.01
	LC - 16 reps	0.0005	0.01	0.0005	0.01	0.0005	0.01
Weight Sharing	LC - ws(1)	0.001	0.01	0.001	0.0001	0.001	0.01
	LC - ws(10)	0.0005	0.01	0.0005	0.01	0.001	0.0001
	LC - ws(100)	0.0005	0.01	0.0005	0.01	0.001	0.01

Table 12: Hyperparameters for padding of 8.

Regularizer	Connectivity	CIFAR10		CIFAR100		TinyImageNet	
		Learning rate	Weight decay	Learning rate	Weight decay	Learning rate	Weight decay
-	conv	0.01	0.01	0.01	0.01	0.005	0.01
	LC	0.001	0.01	0.0005	0.0001	0.001	0.01
Data Translation	LC - 4 reps	0.0005	0.01	0.001	0.0001	0.0005	0.01
	LC - 8 reps	0.001	0.01	0.0005	0.0001	0.0005	0.0001
	LC - 16 reps	0.0005	0.0001	0.0005	0.01	0.0005	0.01
Weight Sharing	LC - ws(1)	0.001	0.0001	0.001	0.01	0.001	0.01
	LC - ws(10)	0.0005	0.01	0.0005	0.0001	0.001	0.0001
	LC - ws(100)	0.0005	0.01	0.0005	0.0001	0.001	0.0001

Table 13: Performance of convolutional (conv), locally connected (LC) and locally connected with convolutional first layer (LC + 1st layer conv) networks on ImageNet (1 run). For LC, we also used dynamic weight sharing every n batches. LC nets additionally show performance difference w.r.t. the conv net.

Model	Connectivity	Weight sharing frequency	ImageNet			
			Top-1 accuracy (%)	Diff	Top-5 accuracy (%)	Diff
0.5x ResNet18	conv	-	63.5	-	84.7	-
	LC	-	46.7	-16.8	70.0	-14.7
	LC	1	61.7	-1.8	83.1	-1.6
	LC	10	59.3	-4.2	81.1	-3.6
	LC	100	54.5	-9.0	77.7	-7.0
0.5x ResNet18 (1st layer conv)	LC	-	52.2	-11.3	75.1	-9.6
	LC	1	63.6	0.1	84.5	-0.2
	LC	10	61.6	-1.9	83.1	-1.6
	LC	100	59.1	-4.4	81.1	-3.6